nature photonics

Article

https://doi.org/10.1038/s41566-022-01100-0

Nonlinear helical dichroism in chiral and achiral molecules

In the format provided by the authors and unedited

Supplementary materials: Nonlinear helical dichroism in chiral and achiral molecules

Jean-Luc Bégin[1,+], Ashish Jain[1,+], Andrew Parks[1], Felix Hufnagel[1], Paul Corkum[1], Ebrahim Karimi[1], Thomas Brabec[1], and Ravi Bhardwaj[1,*]

[1]Department of Physics, University of Ottawa, Ottawa, ON, K1N 6N5, Canada

Contents

1 HD(Type I, II) in limonene and fenchone

Figures S1 shows HD(Type II) in limonene as a function of fluence for $l = \pm 1$ (Fig.S1a) and ± 3 (Fig.S1b) , respectively for linearly poarized helical light. The chiral signal increases with laser fluence and reaches a maximum of $\sim$ 6-7%. The chiral signals in limonene and fenchone are of opposite signs (black curve and red curves are flipped) because they rotate the plane of linear polarization in opposite directions *(see Methods)*. The chiral signal did not increase with l-value in limonene.

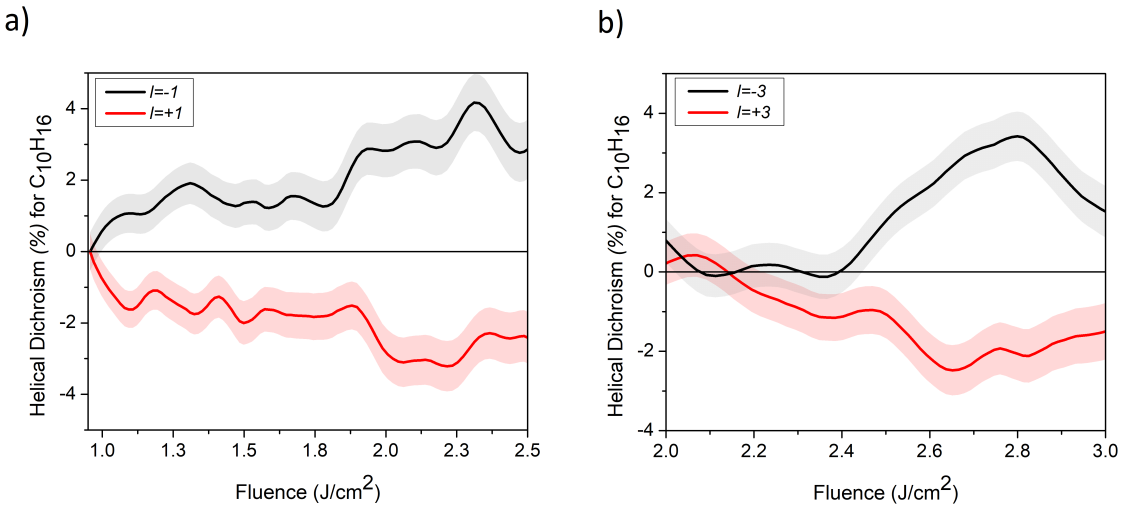

FIG. S 1. HD(Type II) in limonene with linearly polarized light ($s = 0$) as a function of peak laser fluence. **(a)** $l = \pm 1$. **(b)** $l = \pm 3$. The colour bands represent the propagation error of the chiral signal for three independent measurements (sample size).

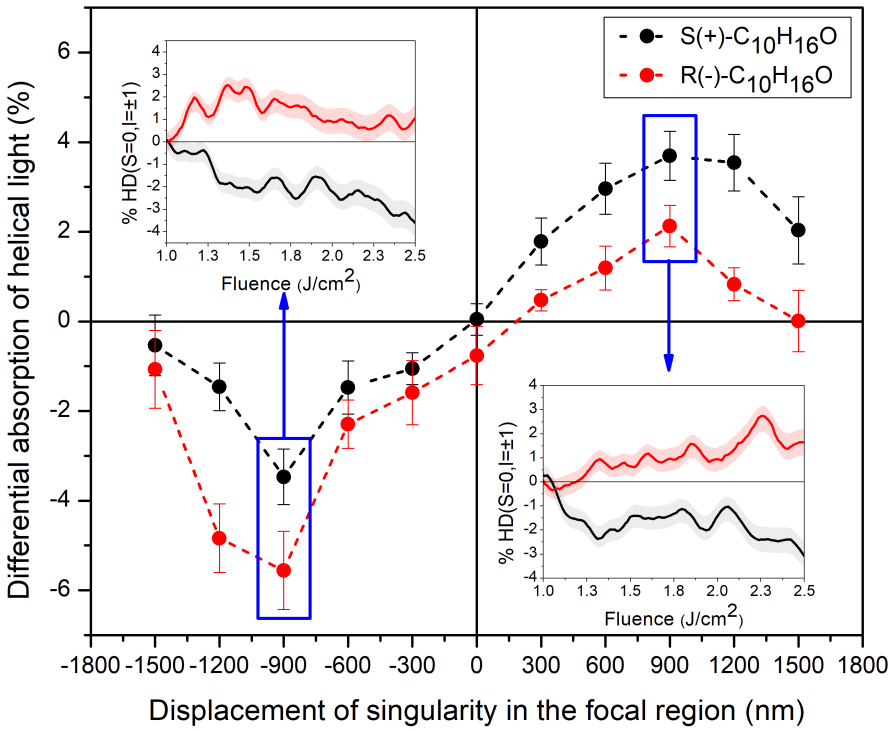

FIG. S 2. Helical dichroism with asymmetric OAM beams in fenchone. Differential absorption of linearly polarized helical light $l = \pm 1$ as a function of the position (or displacement) of the singularity in the OAM beam. The insets show helical dichroism as function of peak laser fluence when the singularity is at the positions marked by solid rectangles. The error bars and colour bands represent the propagation error of the chiral signal for three independent measurements (sample size).

Figure. S2 shows that HD signal in fenchone. The spatial variation of differential absorption, HD(Type I), of linearly polarized helical light in fenchone enantiomers exhibits the same behaviour as achiral molecules (Fig. 3b) as well as limonene enantiomers (Fig. 4). The insets of Fig. S2 represent HD(Type II) as a function of peak laser fluence when the singularity was at the positions marked by solid rectangles.

2 Intensity profile of OAM beams before and after the sample

To ensure that the beam profile is not influenced by nonlinear propagation effects at the interaction region we took single shot images of the beam profile with and without the sample as shown in fig. S3. A pulse energy of 350 nJ for $l = \pm 1$ was chosen because the magnitude helical dichroism (see main article) is largest around that energy region. There was no change in the beam profile after propagating through the sample. This suggests the nonlinear absorption is not influenced by any propagation effects.

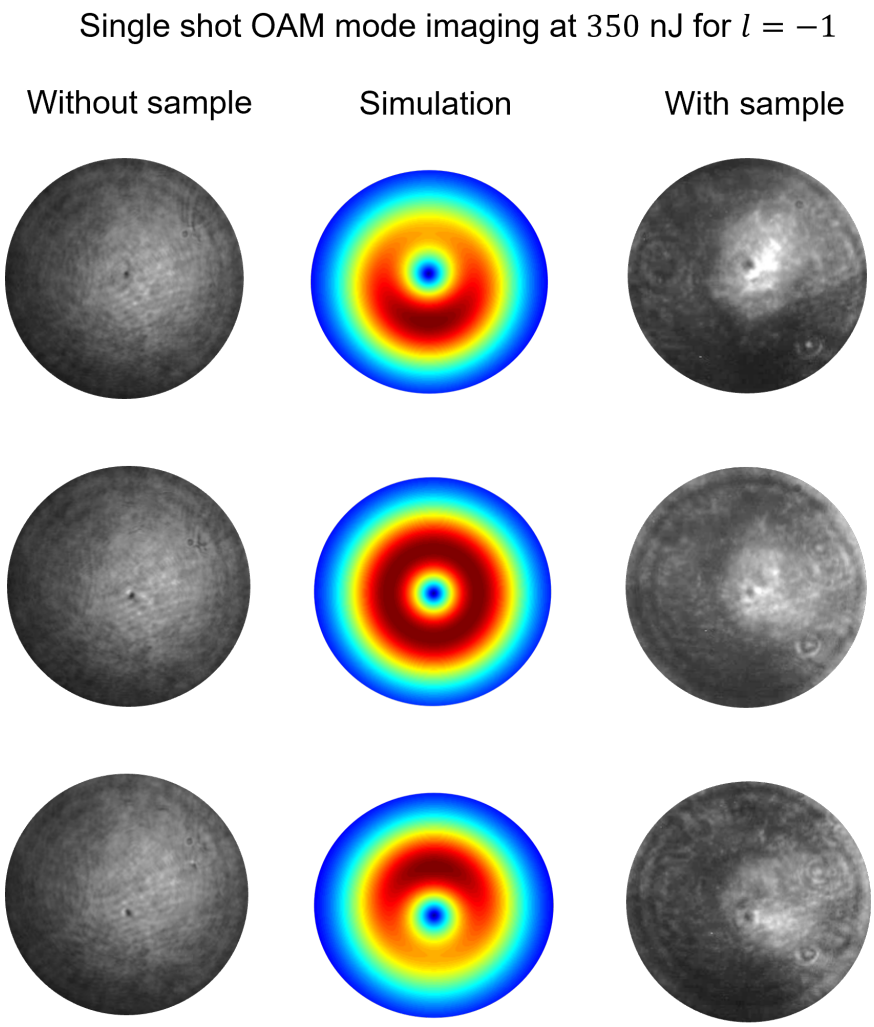

FIG. S 3. Single shot beam profiles of $l = -1$ for a symmetrical LG (center row) and asymmetrical LG (top and bottom rows) beams. The left (right) column shows the beam profiles without(with) the sample. The central column shows the simulated intensity profiles.

3 Measuring the transmitted l value of an OAM beam

To ensure the l value remained unchanged after propagating through the sample, we performed a set of interference experiments involving Gaussian and OAM beams to observe the signature fork patterns. Fig. S4 depicts simulated and measured single-shot fork patterns for $l = -1$ in air (a,b) , $l = +3$ in sample (c,d). Fig. S4 e,f shows the measured patterns for $l = \pm 1$ in the sample. Though the contrast of the interference patterns is poor in the sample due to single-shot measurement, they are in agreement with the expected signature patterns. Results indicate no change in the angular momentum value of the light when propagating through the sample.

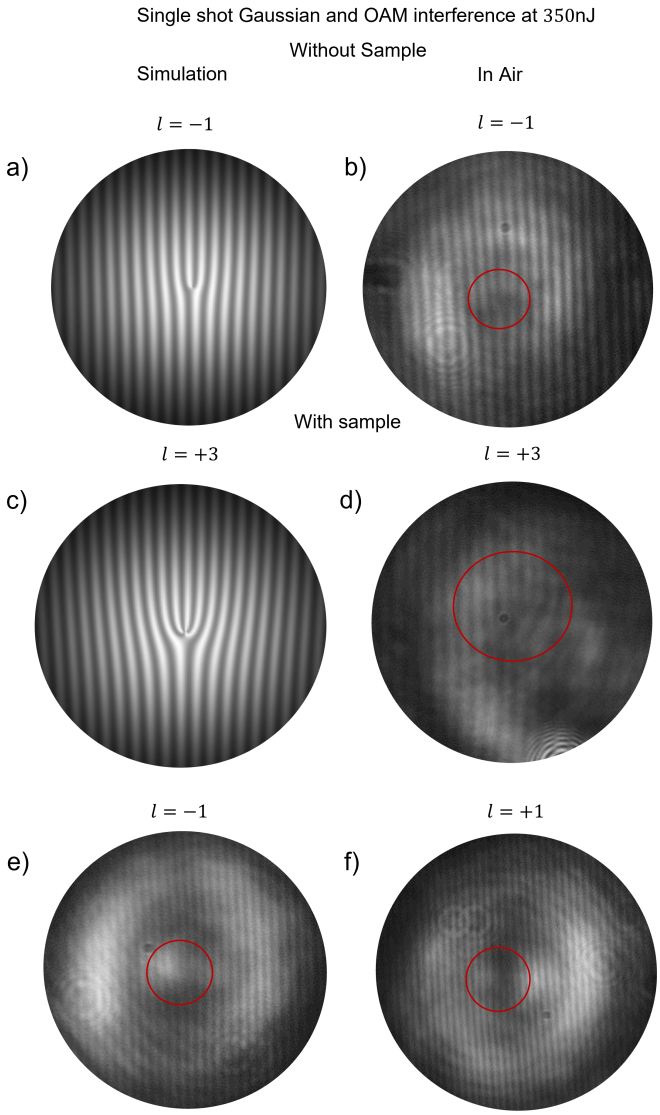

FIG. S 4. Simulated and measured (a,b) two pronged fork pattern for $l = -1$ in air, (c,d) four pronged fork pattern for $l = +3$ in sample. (e,f) measured two pronged fork pattern for $l = \pm 1$ in sample.

4 Single shot transmitted spectrum measurement

Nonlinear affects such as self-phase modulation can influence the propagation of incident light through the sample over the range of pulse energies used in the experiment. Fig. S5 shows set of single-shot spectra (a) of Ti: Sapphire laser used as a reference (black curve), (b) after the power and OAM/SAM control optics (magenta curve) with no sample, and (c) after propagating through (-)-fenchone and (+)-fenchone for linearly polarized helical light, $+l$ (cyan and green curves, respectively) and $-l$ (red and blue curves, respectively). There is no considerable change in the spectral shape after propagating through the sample suggesting nonlinear affects are negligible. Compared to the reference spectrum, the spectrum of light incident on the sample is altered due to numerous optics in the beam path.

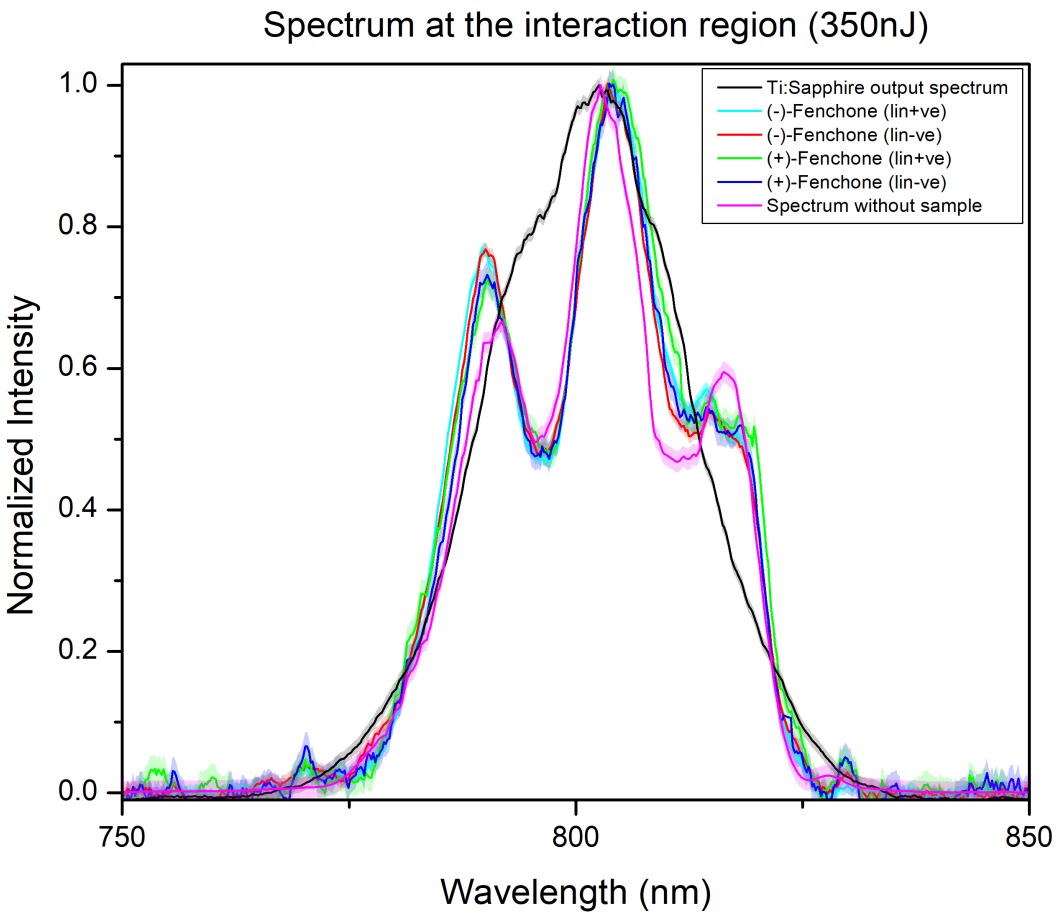

FIG. S 5. Single-shot measurement of transmitted spectra. The reference spectrum (black curve) corresponds to Ti:sapphire laser, spectrum after the power and OAM/SAM contol but with no sample (magenta curve). The cyan (green) and red (blue) curves are the spectrum of linearly polarized $l = +1$ (lin +ve) and $l = -1$ (lin -ve) after propagating through (-)-fenchone ((+)-fenchone).

5 Transmission measurements in air in the absence of sample

In the absence of a sample, transmission measurements conducted in air ensure that the photodiodes detect identical signals when changing the incoming linearly polarized light from $+l$ to $-l$. Fig. S6 a) and b) show transmission of a symmetrical and an asymmetrical LG beams through air. The red (black) curves represent the difference between the PD1 (PD2) signal for linearly polarized $+l$ and $-l$. Both signals are centered about zero with a fluctuation of $\pm 0.05V$. Moreover, the red and black curves nearly overlap over the entire energy range, demonstrating no signal change between PD1 (incident light) and PD2 (transmitted light) as the OAM value changed. This indicates there is no arbitrary signal/noise introduced by the experimental setup to the observed differential absorption in chiral and achiral molecules. Transmission measurements in air were performed before every experimental run and for every position of the displaced singularity.

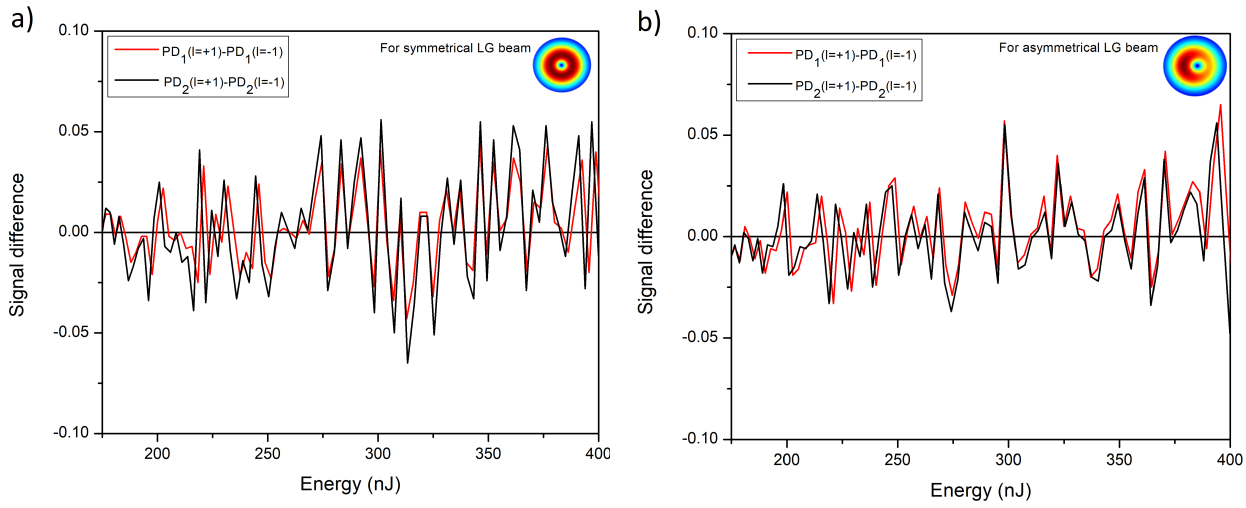

FIG. S 6. Transmission linearly polarized helical light in air (no sample) (a) for a symmetrical and (b) asymmetrical LG beams. The red (black) curve represents the difference between the PD1 signal for $+l$ and $-l$ (PD2 monitoring the transmitted light).

6 Differential absorption with non-OAM beams

Figure S7a shows normalized transmission of a linearly polarized Gaussian beam propagating through left- and right-handed chiral molecule. Both in the linear and the nonlinear regimes, the two curves overlap exhibiting no differential absorption. Similar transmission measurements were conducted for S(-)-limonene with left- and right-circularly polarized annular beam resembling an Airy pattern obtained through Fresnel diffraction (Fig. S7b). In absence of phase, which is responsible for orbital angular momentum, there is no differential absorption in a chiral molecule for a beam with a null intensity at the center. The results remained the same even when the null intensity regions was displaced from the center (fig 3c of the main article). This suggests that differential absorption is not purely due to the field gradient. Helical phase plays a crucial role.

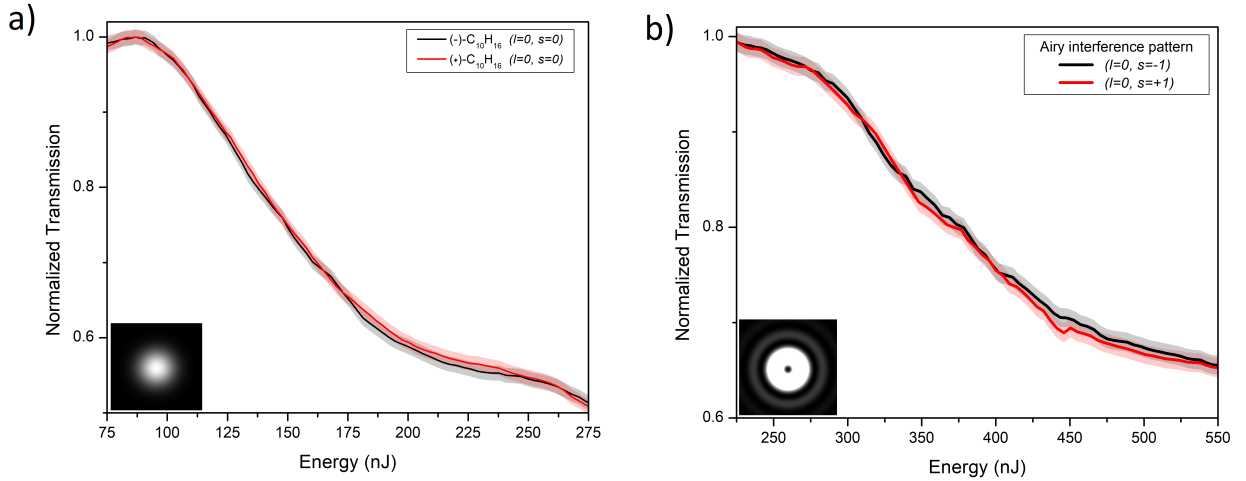

FIG. S 7. (a) Transmission of linearly polarized Gaussian in left- and right-handed limonene. (b) Transmission of left- and right-circularly polarized annular non-OAM beam for S(-)-limonene. Insets show the beam profiles. The colour bands represent the propagation error of the chiral signal for three independent measurements (sample size).

7 Spatial Mapping of singularity

Fig. S8 shows 2D contour map of differential absorption of linearly polarized (ε= 0.09) left and right handed OAM ($l = \pm 1$) for (+)-fenchone, obtained by displacing the singularity in the xy plane. The results presented in Fig.3, 4 (main text) and Fig. S2 are a line scan along one axial direction. The sinusoidal behaviour of differential absorption becomes asymmetric as we displace our singularity off-axis. This behaviour is likely due to the relative angle between the polarization direction and the direction of displacement of the singularity.

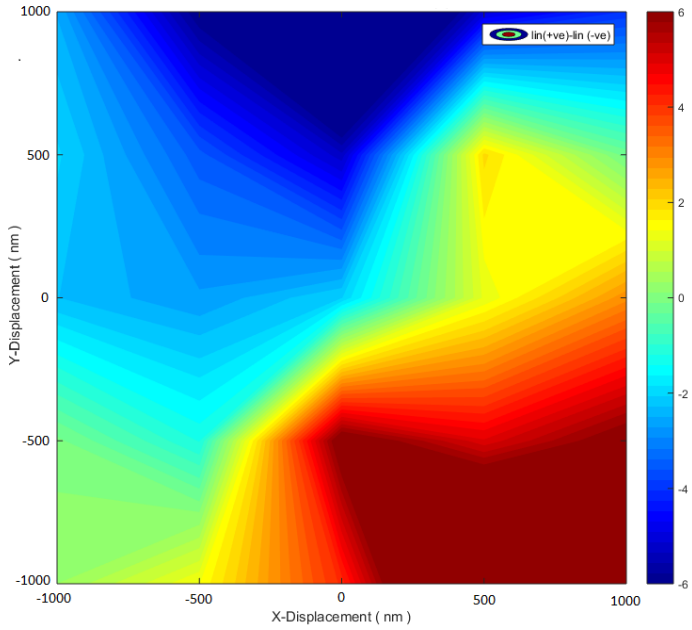

FIG. S 8. Differential absorption of linearly polarized helcial light ($l = \pm 1$) in (+)-fenchone as a function of the displacement of the singularity in the XY-plane.

8 Fluence calculations

In LG beams with increasing l-value, the size of the null intensity region at the center increases. Consequently, for the same spot size higher pulse energies are required to reach the threshold for the onset of nonlinear absorption. This can be seen from the transmission curves shown in Fig. S9 for $l = 1$ (left) and $l = 3$ (right) plotted as a function of laser pulse energy in fenchone.

From the threshold energies, the peak fluence is calculated based on the below equation[1]:

$$F_l\left[\frac{J}{(cm^2)}\right] = \frac{2^{(|l|+1)} r^{2|l|} e^{\frac{-2r^2}{\omega(z)^2}}}{|l|!\pi\omega(z)^{2(|l|+1)}} E_l^{th}[J]$$

where $l = 0; \pm 1; \pm 2; \pm 3\ldots$ is the orbital angular momentum value, r is the radial direction, $\omega(z)$ is the radius of a beam evaluated at z=0 and E_l is the threshold pulse energy for different l-values.

For peak fluence, radial parameter r is evaluated at the mamxima of the intensity profile. For Gaussian beam ($l = 0$) maxima occurs at r = 0, for OAM beam with $l = 1$ at $r_{pk} = \pm\frac{w_0}{\sqrt{2}}$ and subsequently for higher order l values at the position of their respective maxima.

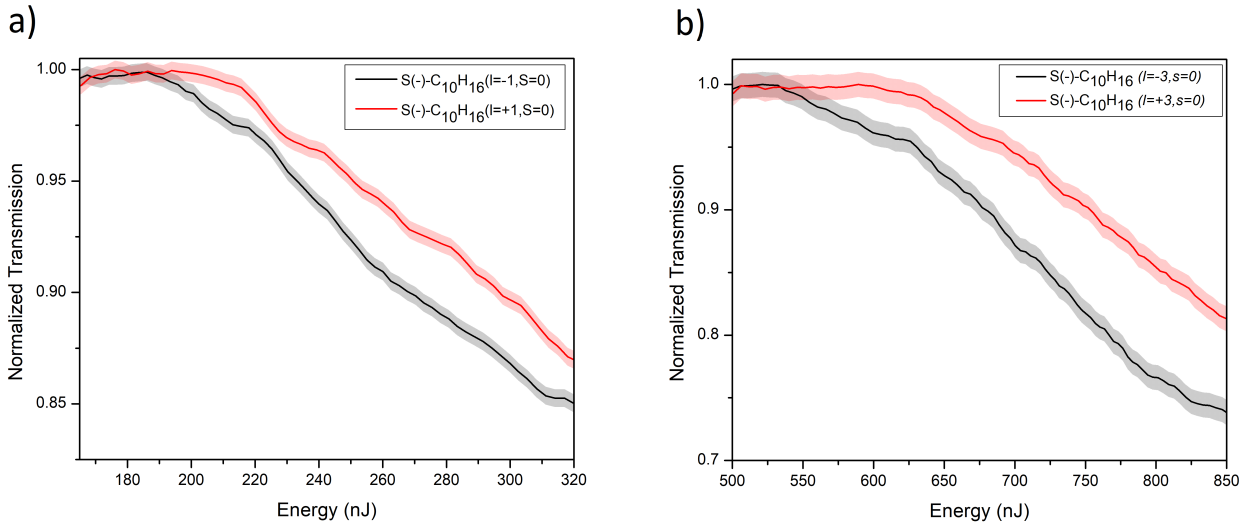

FIG. S 9. Transmission curves of limonene with linearly polarized light ($s = 0$) as a function of pulse energy. **(a)** $l = \pm 1$. **(b)** $l = \pm 3$. The colour bands represent the propagation error of the chiral signal for three independent measurements (sample size).

Substituting the above values for radial parameter, we get

$$\text{For } l = 0 \text{ beam} : F_0\left(r_{pk}\right) = 2\frac{E_0^{th}}{\pi w_0^2}$$

$$\text{For l = 1 beam} : F_1\left(r_{pk}\right) = 2e^{-1}\frac{E_1^{th}}{\pi w_0^2}$$

One can obtain similar equations for higher order OAM beams from which the peak laser fluences were calculated for the presented results.

9 Optical dipole force

Here we show that optical gradient forces are non-zero for asymmetric LG beams. The total force acting on a dipole can be written as[2]

$$\mathbf{F} = (\mu \cdot \nabla)\mathbf{E} + \dot{\mu} \times \mathbf{B} + \dot{\mathbf{r}} \times (\mu \cdot \nabla)\mathbf{B} \tag{1}$$

where μ is the dipole moment. Here first term on the RHS containing the inner product$(\mu \cdot \nabla)$ represents the dipole force due to inhomogeneity in the fields. Second term is the expression of standard Lorentz force and third term represents particle movement in the inhomogeneous magnetic field. The above equation was obtained by assuming dipoles does not change the incident fields. For non relativistic speeds ($\dot{r} << c$), third term can be neglected as it is much smaller in comparison to first two terms. Substituting $\mu = \alpha(\omega)\mathbf{E}(\mathbf{r})$ where α is atomic polarizability, we get,

$$\mathbf{F} = \alpha(\mathbf{E} \cdot \nabla)\mathbf{E} + \alpha(\frac{d\mathbf{E}}{dt} \times \mathbf{B}) \tag{2}$$

Using vector identity $(\mathbf{E} \cdot \nabla)\mathbf{E} = \frac{1}{2}\nabla\left(E^2\right) - \mathbf{E} \times (\nabla \times \mathbf{E})$ and second maxwell equation we get,

$$\mathbf{F} = \alpha\frac{1}{2}\nabla E^2 + \alpha\frac{d}{dt}(\mathbf{E} \times \mathbf{B}). \tag{3}$$

Here, first term defines the gradient force and second term is the scattering force which can be neglected when the poynting vector does not change over an optical cycle. Fig. S10 shows the gradient force component (F_x) integrated over the beam

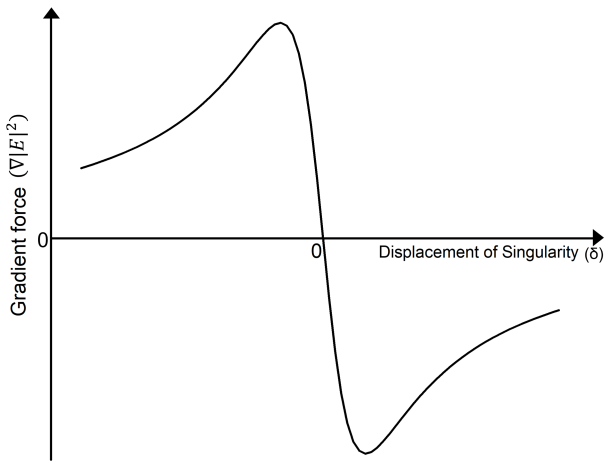

FIG. S 10. Optical gradient force as a function of displaced position of singularities. Optical gradient force is zero for symmetric LG beam and maximum at the position of displaced singularity. Force converges towards zero for the extreme displacement in singularity where beam profile mimics gaussian profile.

cross-section as a function of displaced position of the singularity. For linearly polarized light one of the transverse components will be dominant. The F_y component would be smaller in magnitude however exhibits similar behaviour. The gradient force is zero for the symmetric LG beam for which the singularity is at the center. When the singularity is displaced, the gradient forces initially increases and then decreases to zero for large displacement. A non-zero gradient force would give rise to a torque which preferentially aligns the molecular axis parallel the polarization plane[3]. Such alignment of molecules in an asymmetric LG beams will lead to non-zero averaged E1E2 dipole-quadrupole contribution to HD. Therefore, the HD signal, shown in Fig. 5 of the main text, is zero for symmetric LG beams, increases with the displacement of the singularity reaching a maximum and then decreases when the singularity reaches the beam periphery.

10 Extension of theory to multiphoton case using time-dependent perturbation theory

Using perturbation theory, a generic time-dependent wavefunction

$$|\Psi\rangle = |\Psi\rangle^{(0)} + \sum_m c_m(t)\,|\Psi_m\rangle^{(0)} \tag{4}$$

satisfies the Schrodinger equation

$$(H_0 + \lambda V(t))\,|\Psi\rangle = i\hbar\frac{\partial}{\partial t}|\Psi\rangle \tag{5}$$

where, λ is the perturbation parameter and

$$V(t) = -\mu_\alpha E_\alpha - \frac{1}{3}\theta_{\alpha\beta}\nabla_\alpha E_\beta - m_\alpha B_\alpha - \ldots \tag{6}$$

is the interaction Hamiltonian[4,5]. The corresponding multipoles and fields are complex quantities. $|\Psi\rangle^{(0)} = |\psi\rangle^{(0)} e^{-iE_n^{(0)}t/\hbar}$ are the stationary states satisfying

$$H_0|\Psi\rangle^{(0)} = i\hbar\frac{\partial}{\partial t}|\Psi\rangle^{(0)} \tag{7}$$

We can expand the time dependent coefficient $c_m(t)$ in powers of perturbation parameter λ.

$$c_m(t) = c_m^{(0)} + \lambda c_m^{(1)}(t) + \lambda^2 c_m^{(2)}(t) + ... + \lambda^n c_m^{(n)}(t) \tag{8}$$

where different order coeffecients can be obtained by comparing powers of perturbation parameter λ

$$c_m^{(0)} t(t) = \left(\frac{1}{i\hbar}\right) \int_{-\infty}^{t} dt' \langle m|V(t')|g\rangle e^{i\omega_{mg}t} \tag{9}$$

and nth order is defined as,

$$c_m^{(n)}(t) = \left(\frac{1}{i\hbar}\right)^n \sum_l \int_{-\infty}^{t} dt' \langle m|V(t')|l\rangle c_l^{(n-1)}(t') e^{i\omega_{ml}t'} \tag{10}$$

Now, we calculate the single photon absorption rate and generalize it to multiphoton absorption[6] Considering a interaction Hamiltonian of the form

$$V(t) = Ve^{-i\omega t} + V^* e^{i\omega t} \tag{11}$$

By implementing the rotating wave approximation, we neglected the complex conjugate of the field because we are only considering absorption and ignore the stimulated emission (anti-resonant terms). The probability amplitude can be expressed as

$$p_m^{(n)}(t) = |c_m^{(n)}(t)|^2 \tag{12}$$

and the rate of transition

$$R_{mg}^{(n)} = \frac{p_m^{(n)}(t)}{t} \tag{13}$$

therefore, for single photon we obtain Fermi's golden rule

$$R_{mg}^{(1)} = \frac{2\pi}{\hbar^2} |\langle m|V|g\rangle|^2 \delta(\omega_{mg} - \omega) \tag{14}$$

Single photon transition rate is proportional to absorption cross-section[6] which is proportional to the rate of energy absorption (Γ) derived in the main text. Substituting the interaction Hamiltonian into the rate expression, we get

$$R_{mg}^{(1)} = \frac{2\pi}{\hbar^2} |-\mu_\alpha^{mg} E_\alpha - \frac{1}{3}\theta_{\alpha\beta}^{mg} \nabla_\alpha E_\beta - m_\alpha^{mg} B_\alpha|^2 \delta(\omega_{mg} - \omega) \tag{15}$$

For physical situations, the delta function can be replaced by a lineshape function

$$R_{mg}^{(1)} = \frac{2\pi}{\hbar^2} |-\mu_\alpha^{mg} E_\alpha - \frac{1}{3}\theta_{\alpha\beta}^{mg} \nabla_\alpha E_\beta - m_\alpha^{mg} B_\alpha|^2 \rho(\omega_{mg} = \omega) \tag{16}$$

$$\begin{aligned} R_{mg}^{(1)} = \frac{2\pi}{\hbar^2} \Bigg(& \left(\mu_\alpha^{mg} E_\alpha\right)\left(\mu_\alpha^{mg} E_\alpha\right)^* + \left(\mu_\alpha^{mg} E_\alpha\right)\left(m_\alpha^{mg} B_\alpha\right)^* + \left(\mu_\alpha^{mg} E_\alpha\right)\left(\frac{1}{3}\theta_{\alpha\beta}^{mg} \nabla_\alpha E_\beta\right)^* + \left(m_\alpha^{mg} B_\alpha\right)\left(\mu_\alpha^{mg} E_\alpha\right)^* \\ & + \left(m_\alpha^{mg} B_\alpha\right)\left(\frac{1}{3}\theta_{\alpha\beta}^{mg} \nabla_\alpha E_\beta\right)^* + \left(m_\alpha^{mg} B_\alpha\right)\left(m_\alpha^{mg} B_\alpha\right)^* + \left(\frac{1}{3}\theta_{\alpha\beta}^{mg} \nabla_\alpha E_\beta\right)\left(\mu_\alpha^{mg} E_\alpha\right)^* + \left(\frac{1}{3}\theta_{\alpha\beta}^{mg} \nabla_\alpha E_\beta\right)\left(m_\alpha^{mg} B_\alpha\right)^* \\ & + \left(\frac{1}{3}\theta_{\alpha\beta}^{mg} \nabla_\alpha E_\beta\right)\left(\frac{1}{3}\theta_{\alpha\beta}^{mg} \nabla_\alpha E_\beta\right)^* \Bigg) \rho(\omega_{mg} = \omega) \end{aligned}$$

Ignoring the M1M1, M1E2 and the E2E2 coupling terms and applying the anisotropic averaging, we get

$$\begin{aligned} R_{mg}^{(1)} = \frac{2\pi}{\hbar^2} \Big[& |\mu_\alpha^{mg}|^2 |E_\alpha|^2 + |m_\alpha^{mg}|^2 |B_\alpha|^2 + \langle \mu_\alpha^{mg} m_\alpha^{mg*} \rangle_\rho (E_\alpha B_\alpha^*) + \langle m_\alpha^{mg} \mu_\alpha^{mg*} \rangle_\rho (B_\alpha E_\alpha^*) \\ & + \frac{1}{3} \left(\langle \theta_{\alpha\beta}^{mg} \mu_\alpha^{mg*} \rangle_\rho \left(\nabla_\alpha E_\beta \cdot E_\alpha^*\right) + \langle \mu_\alpha^{mg} \theta_{\alpha\beta}^{mg*} \rangle \left(E_\alpha \nabla_\alpha E_\beta^*\right) \right) \rho(\omega_{mg} = \omega) \end{aligned}$$

Here ρ is the orientation-dependent weighting factor arising from the anisotropic averaging ($\rho = 0$ for random orientations and $\rho = 1$ for full alignment of molecules). The dipole transition μ is a real quantity , magnetic transition dipole m is imaginary[7]. Approximating the response of the quadrupole tensor as a scalar we can rewrite the above expression as:

$$R_{mg}^{(1)} = \frac{2\pi}{\hbar^2}\left[|\mu_\alpha^{mg}|^2|E_\alpha|^2 + |m_\alpha^{mg}|^2|B_\alpha|^2 + \langle\mu_\alpha^{mg}m_\alpha^{gm}\rangle_\rho\left(B_\alpha E_\alpha^* - E_\alpha B_\alpha^*\right)\right.$$
$$\left. + \frac{1}{3}\left(\langle\mu_\alpha^{mg}\theta_{\alpha\beta}^{gm}\rangle_\rho\left(\nabla_\alpha E_\beta E_\alpha^* + E_\alpha\nabla_\alpha E_\beta^*\right)\right)\right]\rho\left(\omega_{mg} = \omega\right)$$

Since $B_\alpha E_\alpha^* - E_\alpha B_\alpha^* = -2iIm\left[E_\alpha^* B_\alpha\right]$ and, $\left(E_\alpha^*\nabla_\alpha E_\beta + E_\alpha\nabla_\alpha E_\beta^*\right) = 2\mathrm{Re}\left[E_\alpha^*\nabla_\alpha E_\beta\right]$ we can rewrite the above expression as

$$R_{mg}^{(1)} = \frac{2\pi}{\hbar^2}\left[\underbrace{|\mu_\alpha^{mg}|^2|E_\alpha|^2}_{\mathrm{E1E1}} + \underbrace{|m_\alpha^{mg}|^2|B_\alpha|^2}_{\mathrm{M1M1}} + \underbrace{2\langle\mu_\alpha^{mg}m_\alpha^{gm}\rangle_\rho\mathrm{Im}\left[E_\alpha^*B_\alpha\right]}_{\mathrm{E1M1}} + \underbrace{\frac{2}{3}\langle\mu_\alpha^{mg}\theta_{\alpha\beta}^{gm}\rangle_\rho\mathrm{Re}\left[E_\alpha^*\nabla_\alpha E_\beta\right]}_{\mathrm{E1E2}}\right]\rho\left(\omega_{mg} = \omega\right) \tag{17}$$

This is the single photon transition rate and resembles equation (8) of main text. $\mathrm{Im}\left[E_\alpha^*B_\alpha\right]$ and $\mathrm{Re}\left[E_\alpha^*\nabla_\alpha E_\beta\right]$ correspond to optical chirality C and helicity Υ, respectively.

The transition rate for two photon process (transition states: g $\rightarrow k \rightarrow m$) is

$$R_{mg}^{(2)} = 2\pi\left|\sum_k \frac{V_{mk}V_{kg}}{\hbar^2\left(\omega_{kg} - \omega\right)}\right|^2\rho\left(\omega_{mg} = 2\omega\right) \tag{18}$$

$$R_{mg}^{(2)} = 2\pi\left|\sum_k \frac{\left(\mu_\alpha^{mk}E_\alpha + \frac{1}{3}\theta_{\alpha\beta}^{mk}\nabla_\alpha E_\beta + m_\alpha^{mk}B_\alpha\right)\left(\mu_\alpha^{kg}E_\alpha + \frac{1}{3}\theta_{\alpha\beta}^{kg}\nabla_\alpha E_\beta + m_\alpha^{kg}B_\alpha\right)}{\hbar^2\left(\omega_{kg} - \omega\right)}\right|^2\rho\left(\omega_{mg} = 2\omega\right) \tag{19}$$

$$R_{mg}^{(2)} = 2\pi\left|\sum_k \frac{\left(\mu_\alpha^{mk}E_\alpha\right)\left(\mu_\alpha^{kg}E_\alpha\right) + \left(m_\alpha^{mk}B_\alpha\right)\left(\mu_\alpha^{kg}E_\alpha\right) + \left(\mu_\alpha^{mk}E_\alpha\right)\left(m_\alpha^{kg}B_\alpha\right) + \left(\frac{1}{3}\theta_{\alpha\beta}^{mk}\nabla_\alpha E_\beta\right)\left(\mu_\alpha^{kg}E_\alpha\right) + \left(\mu_\alpha^{mk}E_\alpha\right)\left(\frac{1}{3}\theta_{\alpha\beta}^{kg}\nabla_\alpha E_\beta\right)}{\hbar^2\left(\omega_{kg} - \omega\right)}\right|^2\rho\left(\omega_{mg} = 2\omega\right) \tag{20}$$

Ignoring the higher order terms involving M1 and E2 we get

$$R_{mg}^{(2)} = 2\pi\sum_k \frac{1}{\hbar^4\left(\omega_{kg} - \omega\right)^2}\left\{\left|\mu_\alpha^{mk}E_\alpha\right|^2\left|\mu_\alpha^{kg}E_\alpha\right|^2 + \left|\mu_\alpha^{kg}E_\alpha\right|^2\left[\left(\mu_\alpha^{mk}E_\alpha\right)\left(m_\alpha^{mk}B_\alpha\right)^* + \left(m_\alpha^{mk}B_\alpha\right)\left(\mu_\alpha^{mk}E_\alpha\right)^*\right]\right.$$
$$+ \left|\mu_\alpha^{kg}E_\alpha\right|^2\left[\left(\mu_\alpha^{mk}E_\alpha\right)\left(\frac{1}{3}\theta_{\alpha\beta}^{mk}\nabla_\alpha E_\beta\right)^* + \left(\frac{1}{3}\theta_{\alpha\beta}^{mk}\nabla_\alpha E_\beta\right)\left(\mu_\alpha^{mk}E_\alpha\right)^*\right] + \left|\mu_\alpha^{mk}E_\alpha\right|^2\left[\left(\mu_\alpha^{kg}E_\alpha\right)\left(m_\alpha^{kg}B_\alpha\right)^* + \left(m_\alpha^{kg}B_\alpha\right)\left(\mu_\alpha^{kg}E_\alpha\right)^*\right]$$
$$\left. + \left|\mu_\alpha^{mk}E_\alpha\right|^2\left[\left(\mu_\alpha^{kg}E_\alpha\right)\left(\frac{1}{3}\theta_{\alpha\beta}^{kg}\nabla_\alpha E_\beta\right)^* + \left(\frac{1}{3}\theta_{\alpha\beta}^{kg}\nabla_\alpha E_\beta\right)\left(\mu_\alpha^{kg}E_\alpha\right)^*\right]\right\}\rho\left(\omega_{mg} = 2\omega\right)$$

Implementing anisotropic averaging, we get

$$R_{mg}^{(2)} = 2\pi\sum_k \frac{1}{\hbar^4\left(\omega_{kg} - \omega\right)^2}\left\{\left|\mu_\alpha^{mk}\mu_\alpha^{kg}\right|^2|E_\alpha E_\alpha|^2 + \left|\mu_\alpha^{kg}\right|^2|E_\alpha|^2\left[\langle\mu_\alpha^{mk}m_\alpha^{mk*}\rangle_\rho\left(E_\alpha B_\alpha^*\right) + \langle m_\alpha^{mk}\mu_\alpha^{mk*}\rangle_\rho\left(B_\alpha E_\alpha^*\right)\right]\right.$$
$$+ \left|\mu_\alpha^{kg}\right|^2|E_\alpha|^2\left[\langle\mu_\alpha^{mk}\tfrac{1}{3}\theta_{\alpha\beta}^{mk*}\rangle_\rho\left(E_\alpha\nabla_\alpha E_\beta^*\right) + \langle\tfrac{1}{3}\theta_{\alpha\beta}^{mk}\mu_\alpha^{mk*}\rangle_\rho\left(\nabla_\alpha E_\beta E_\alpha^*\right)\right] + \left|\mu_\alpha^{mk}\right|^2|E_\alpha|^2\left[\langle\mu_\alpha^{kg}m_\alpha^{kg*}\rangle_\rho\left(E_\alpha B_\alpha^*\right) + \langle m_\alpha^{kg}\mu_\alpha^{kg*}\rangle_\rho\left(B_\alpha E_\alpha^*\right)\right]$$
$$\left. + \left|\mu_\alpha^{mk}\right|^2|E_\alpha|^2\left[\langle\tfrac{1}{3}\mu_\alpha^{kg}\theta_{\alpha\beta}^{kg*}\rangle_\rho\left(E_\alpha\nabla_\alpha E_\beta^*\right) + \langle\tfrac{1}{3}\theta_{\alpha\beta}^{kg}\mu_\alpha^{kg*}\rangle_\rho\left(\nabla_\alpha E_\beta E_\alpha^*\right)\right]\right\}\rho\left(\omega_{mg} = 2\omega\right)$$

$$R_{mg}^{(2)} = 2\pi\sum_k \frac{1}{\hbar^4\left(\omega_{kg} - \omega\right)^2}\left\{\left|\mu_\alpha^{mk}\mu_\alpha^{kg}\right|^2|E_\alpha E_\alpha|^2 + 2\left(\left|\mu_\alpha^{kg}\right|^2|E_\alpha|^2\langle\mu_\alpha^{mk}m_\alpha^{km}\rangle_\rho + \left|\mu_\alpha^{mk}\right|^2|E_\alpha|^2\langle\mu_\alpha^{kg}m_\alpha^{gk}\rangle_\rho\right)\mathrm{Im}\left[E_\alpha^*B_\alpha\right]\right.$$
$$\left. + \tfrac{2}{3}\left(\left|\mu_\alpha^{kg}\right|^2|E_\alpha|^2\langle\mu_\alpha^{mk}\theta_{\alpha\beta}^{km}\rangle_\rho + \left|\mu_\alpha^{mk}\right|^2|E_\alpha|^2\langle\mu_\alpha^{kg}\theta_{\alpha\beta}^{gk}\rangle_\rho\right)\mathrm{Re}\left[E_\alpha^*\nabla_\alpha E_\beta\right]\right\}\rho\left(\omega_{mg} = 2\omega\right)$$

Generalizing for n-photon case, where m is the final state and g is the ground state state

$$R_{mg}^{(n)} = 2\pi \left[\sum_p \sum_l \cdots \sum_r \sum_k \frac{\left| \mu_\alpha^{mp} \mu_\alpha^{pl} \ldots \mu_\alpha^{rk} \mu_\alpha^{kg} \right|^2 |E_\alpha|^{2n}}{\hbar^{2n} \left(\omega_{pl} - (n-1)\,\omega\right)^2 \ldots \left(\omega_{rk} - 2\omega\right)^2 \left(\omega_{kg} - \omega\right)^2} \rho\left(\omega_{mg} = n\omega\right) \right. \tag{21}$$

$$+2 \sum_p \sum_l \cdots \sum_r \sum_k \frac{\left|\mu_\alpha^{mp}\right|^2 \left|\mu_\alpha^{pl}\right|^2 \ldots \left|\mu_\alpha^{rk}\right|^2 \mathrm{Im}\left[\mu_\alpha^{kg} m_\alpha^{gk}\right] + \left|\mu_\alpha^{mp}\right|^2 \left|\mu_\alpha^{pl}\right|^2 \ldots \left|\mu_\alpha^{kg}\right|^2 \langle \mu_\alpha^{rk} m_\alpha^{kr} \rangle_\rho + \ldots +}{\hbar^{2n} \left(\omega_{pl} - (n-1)\,\omega\right)^2 \ldots \left(\omega_{rk} - 2\omega\right)^2 \left(\omega_{kg} - \omega\right)^2} \tag{22}$$

$$\frac{\ldots + \left|\mu_\alpha^{mp}\right|^2 \ldots \left|\mu_\alpha^{rk}\right|^2 \left|\mu_\alpha^{kg}\right|^2 \mathrm{Im}\left[\mu_\alpha^{pl} m_\alpha^{lp}\right] + \left|\mu_\alpha^{pl}\right|^2 \ldots \left|\mu_\alpha^{rk}\right|^2 \left|\mu_\alpha^{kg}\right|^2 \langle \mu_\alpha^{mp} m_\alpha^{pm} \rangle_\rho}{\hbar^{2n} \left(\omega_{pl} - (n-1)\,\omega\right)^2 \ldots \left(\omega_{rk} - 2\omega\right)^2 \left(\omega_{kg} - \omega\right)^2} |E_\alpha|^{2(n-1)} \mathrm{Im}\left[E_\alpha^* B_\alpha\right] \rho\left(\omega_{mg} = n\omega\right) \tag{23}$$

$$+\frac{2}{3} \sum_p \sum_l \cdots \sum_r \sum_k \frac{\left|\mu_i^{mp}\right|^2 \left|\mu_\alpha^{pl}\right|^2 \ldots \left|\mu_\alpha^{rk}\right|^2 \mathrm{Im}\left[\mu_\alpha^{kg} \theta_{\alpha\beta}^{gk}\right] + \left|\mu_\alpha^{mp}\right|^2 \left|\mu_\alpha^{pl}\right|^2 \ldots \left|\mu_\alpha^{kg}\right|^2 \langle \mu_\alpha^{rk} \theta_{\alpha\beta}^{kr} \rangle_\rho + \ldots +}{\hbar^{2n} \left(\omega_{pl} - (n-1)\,\omega\right)^2 \ldots \left(\omega_{rk} - 2\omega\right)^2 \left(\omega_{kg} - \omega\right)^2} \tag{24}$$

$$\left. \frac{\ldots + \left|\mu_\alpha^{mp}\right|^2 \ldots \left|\mu_\alpha^{rk}\right|^2 \left|\mu_\alpha^{kg}\right|^2 \mathrm{Im}\left[\mu_\alpha^{pl} \theta_{\alpha\beta}^{lp}\right] + \left|\mu_\alpha^{pl}\right|^2 \ldots \left|\mu_\alpha^{rk}\right|^2 \left|\mu_\alpha^{kg}\right|^2 \langle \mu_\alpha^{mp} \theta_{\alpha\beta}^{pm} \rangle_\rho}{\hbar^{2n} \left(\omega_{pl} - (n-1)\,\omega\right)^2 \ldots \left(\omega_{rk} - 2\omega\right)^2 \left(\omega_{kg} - \omega\right)^2} |E_\alpha|^{2(n-1)} \mathrm{Re}\left[E_\alpha^* \nabla_\alpha E_\beta\right] \rho\left(\omega_{mg} = n\omega\right) \right] \tag{25}$$

Neglecting the higher order cross terms, we therefore obtain similar expressions involving E1E1, E1M1 and E1E2 expressed in terms of optical chirality C and helicity Υ. The above expressions were obtained in a scalar approximation regime where tensor properties are restricted to a dominant component for oriented molecules. However, when the tensor nature of molecular response is considered there will be multitude of cross terms that arise in case of n-photon transitions whose *l*- dependence needs to be investigated further. We considered n-photon transition rates because in our experiments, for example, interaction of Ti:Sapphire femtosecond laser with limonene (I_P = 8.3 ev) is a 6 photon process.

References

1. Oosterbeek, R., Ashforth, S., Bodley, O., & Simpson, M., Measuring the ablation threshold fluence in femtosecond laser micromachining with vortex and Bessel pulses. *Opt. Express* **26**, 34558-34568 (2018).
2. Novotny, L., & Hecht, B., *Principles of Nano-Optics (2nd ed.)* (Cambridge University Press., 2012).
3. Bradshaw, D. S., & Andrews, D. L., Manipulating particles with light: radiation and gradient forces. *Eur. J. Phys.* **38**, 034008 (2017).
4. Jackson, J. D., *Classical Electrodynamics* (International Adaptation, ISBN: 978-1-119-77077-0, 2021).
5. Barron, L.D.,*Molecular Light Scattering and Optical Activity* (Cambridge University Press, Cambridge, England, 2004).
6. Boyd, R.W., *Nonlinear Optics (3rd ed.)* (Academic Press, 2020).
7. Craig, D. P., & Thirunamachandran, T., *Molecular Quantum Electrodynamics: An introduction to radiation molecule interactions* (Academic Press Inc. London, 1984).